ELSEVIER

Journal of Structural Geology 30 (2008) 50–64

JOURNAL OF STRUCTURAL GEOLOGY

www.elsevier.com/locate/jsg

Spatial distribution of brittle strain in layered sequences

Martin W. Putz-Perrier*, David J. Sanderson

Department of Earth Science and Engineering, Imperial College London, Exhibition Road, London SW7 2AZ, UK

Received 30 March 2007; received in revised form 18 October 2007; accepted 22 October 2007
Available online 12 November 2007

Abstract

A new method of spatial analysis of brittle deformation is proposed that can be applied to both opening mode fractures (joints and veins) and faults. The method has been developed to provide a measure of heterogeneity based on both the position and displacement of individual fractures sampled along a linear traverse. It is based on a non-parametric comparison of the cumulative frequency and strain with that for a uniform distribution. In addition the method provides a statistic that may be used to test a cumulative data-set for significant departures from a uniform distribution.

Two areas of lower Jurassic strata in England provide exceptional outcrops of several kilometre lengths displaying groups of tensile fractures (veins) and normal faults with displacements ranging over 5 to 6 orders of magnitude. The strata consist of shales interbedded with carbonates (decimetres to metres thick), having shale/carbonate ratios of 5/1 and 13/1. Data collected along 25 scan-lines of different length and resolution were analysed. The results show that strain is highly localized at the vein-scale in the more carbonate-rich sequence whilst it is uniformly distributed in the mudstone-dominated sequence. Fault-strain is fairly homogenously distributed in both study areas. These differences may be due to mechanically different behaviours of the sedimentary successions during early deformation history.

Keywords: Strain heterogeneity; Spatial heterogeneity; Brittle strain; Fracture

1. Introduction

Extensional strain in the Upper Crust is heterogeneously distributed and is accommodated by discrete structures such as joints, veins and faults. Each of these groups has been studied individually in much detail (e.g. Segall and Pollard, 1983; Dawers et al., 1993; Vermilye and Scholz, 1995) and our understanding of their mechanical and geometrical properties has increased substantially. What is far less well understood is the spatial distribution of brittle strain accommodated by these different structures, which is the topic of this study.

Due to the restricted resolution and extent of any geological data-set it is difficult to study brittle structures over a large range of scales. Geological observations (e.g. field or seismic studies) only cover small ''windows'', typically of less than two orders magnitude of structure size or displacement, compared to a total scale-range of at least 7 orders of magnitude for both size and displacement in a sedimentary basin. For this reason each group (or scale-range) of structures is usually studied separately from the others, with studies that bring together observations from a wide range of scales being rare (e.g. Bonnet et al., 2001; Putz and Sanderson, in press).

The spatial distribution of fractures strongly influences the permeability (e.g. Renshaw, 1996) and mechanical properties (e.g. Kachanov, 1992; Crampin, 1994) of rocks. An understanding of the distribution of fractures with respect to their size (length and displacement) is essential for analysing subsurface fluid flow, evolution of fracture populations and strain-localization. Much work has been done on quantifying hydraulic properties of faults and fault zones (e.g. Antonellini and Aydin, 1995; Evans et al., 1997; Shipton and Cowie, 2001; Billi et al., 2003). Faults have been demonstrated to act as barriers or conduits for flow, depending on the properties of their fault zone (e.g. Caine et al., 1996; Jourde et al., 2002). The

* Corresponding author.
E-mail address: m_putz@hotmail.com (M.W. Putz-Perrier).

0191-8141/$ - see front matter © 2007 Elsevier Ltd. All rights reserved.
doi:10.1016/j.jsg.2007.10.005

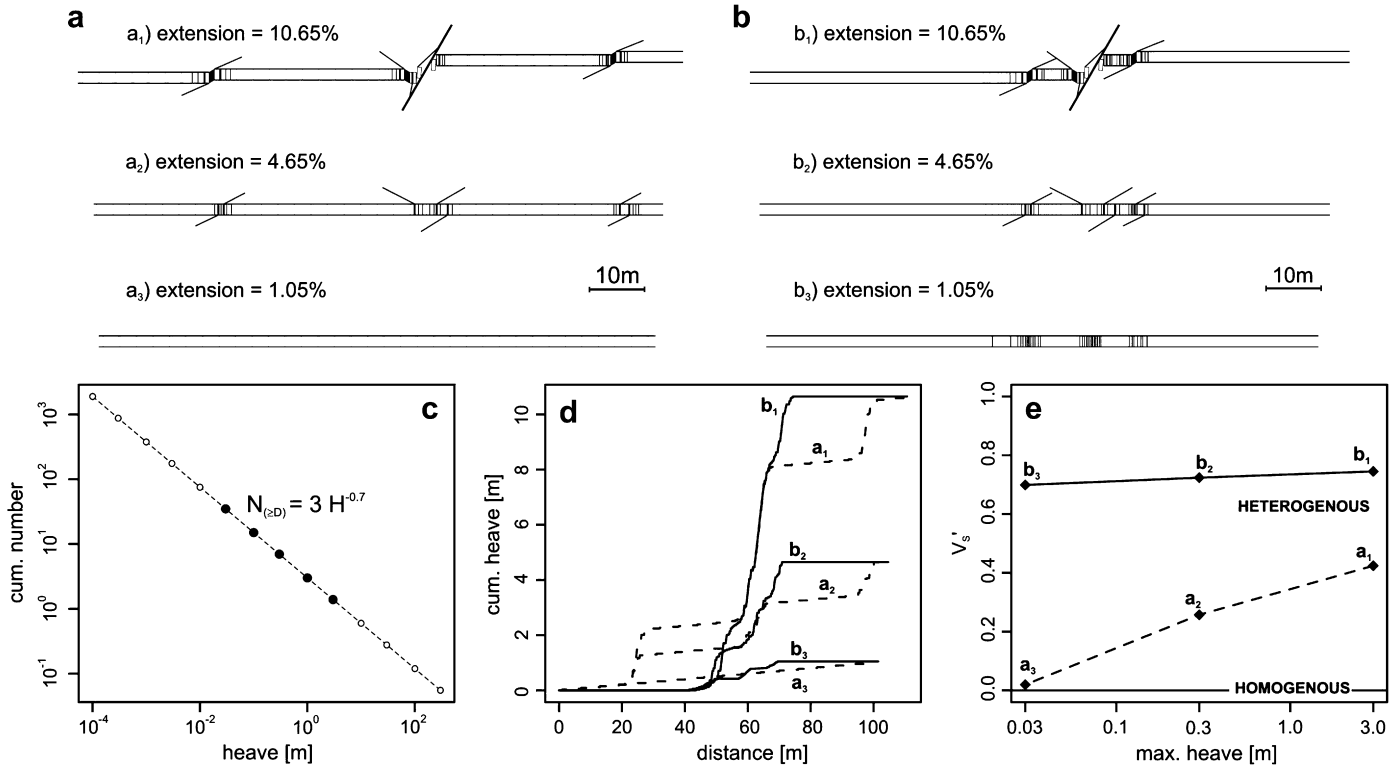

Fig. 1. Examples of spatial strain heterogeneity. (a_1) and (b_1) show layers that have undergone brittle extension by 10.65% accommodated by brittle structures (veins, pull-apart structures and normal faults) with a displacement-size distribution that obeys a power-law as shown in (c). (a_2), (b_2), (a_3) and (b_3) show the same extended layers after removal of the largest-displacement structures. (d) Cumulative heave versus distance plots for examples (a) and (b). (e) Strain heterogeneity V_S' for examples (a) and (b). See text for details.

spatial distribution of fractures (e.g. Gillespie et al., 1993; Gross and Engelder, 1995) may govern the host-rock permeability outside of fault-zones and may cause significant permeability anisotropy (e.g. Renshaw, 1996; Belayneh et al., 2006). Several studies have shown that the presence of joints can increase effective permeability by several orders of magnitude (e.g. Matthäi et al., 1998; Taylor et al., 1999).

Studies dealing with brittle strain and population changes during extension mainly consider faults over restricted scale ranges (e.g. Scholz and Cowie, 1990; Peacock and Sanderson, 1994; Gupta and Scholz, 2000; Bailey et al., 2005). These often use scaling laws to estimate the number and size of structures—and thus the accommodated strain—beyond the observed scale-range (e.g. Marrett and Allmendinger, 1991, 1992; Pickering et al., 1996).

Although scaling relationships are useful for estimating the total strain in a region, they do not provide any information on the spatial distribution of structures and strain.

In the following section we introduce a method that allows the characterization of heterogeneity of strain and fracture spacing at any scale, with the aim of answering three fundamental questions:

1. How is extensional brittle strain distributed in a volume of rock?
2. What are the spatial relationships between faults and veins formed during the same event?
3. How do fracture populations evolve with increasing strain?

2. Method: quantifying spatial heterogeneity from cumulative data

2.1. Coefficient of Variation

The most common method for characterizing the spacing of fracture populations is the determination of the coefficient of variation, which is the ratio of the standard deviation (s) to the mean (m) of the spacing values. For regularly spaced fractures the standard deviation is small ($s < m$), hence $C_V \to 0$; for highly clustered fractures s is large ($s > m$) and $C_V > 1$; for randomly located fractures from a uniform distribution, the spacing values have a negative exponential distribution (see for example Priest, 1993) with $s \approx m$, and hence $C_V \approx 1$. For small samples, it is better to use $C_V^* = C_V((n+1)/(n-1))^{1/2}$, where n is the sample size (Gillespie et al., 2001; Gillespie, 2003). This method has been applied to characterise the spatial evolution of modelled fracture and fault populations (Ackermann et al., 2001; Gillespie et al., 2001). Although the coefficient of variation is useful for analysing fracture spacing, it cannot be adapted easily for the investigation of strain distributions as it does not consider the size of the displacement on the fracture.

2.2. Examples of different strain distribution

Heterogeneity of brittle strain depends on two components: the spatial distribution of the extensional structures (joints,

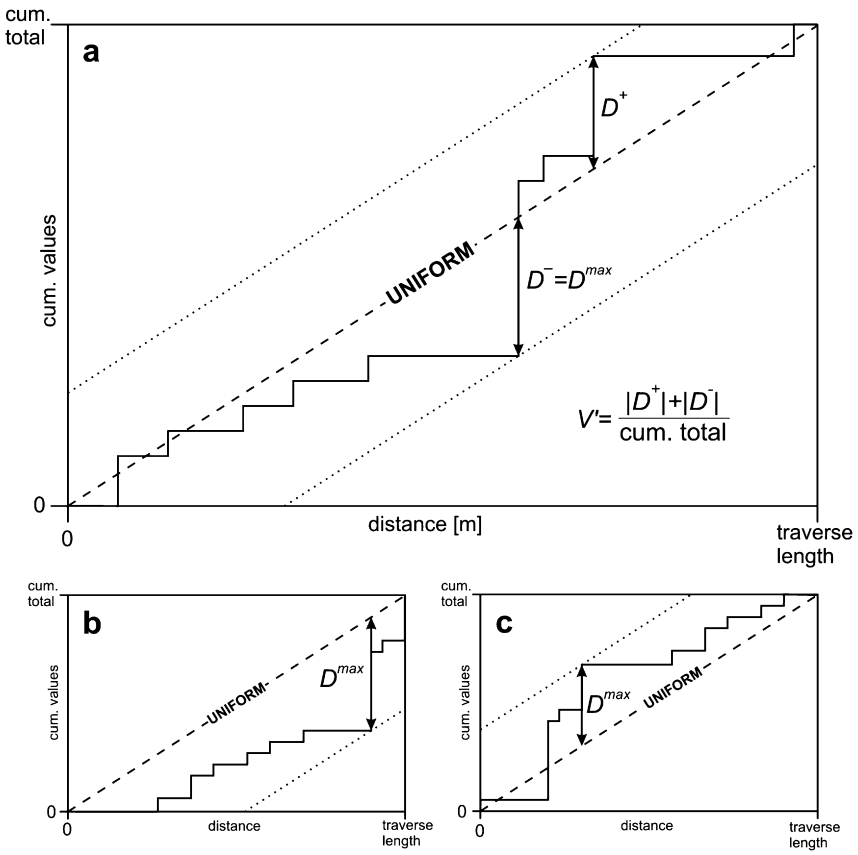

Fig. 2. Kuiper's Test. (a) shows a cumulative graph over distance (solid line). (D^+) and (D^-) are the maximum positive and negative deviations of the cumulative graph from the uniform distribution (dashed line). (b) and (c) show the same cumulative graph as (a) but with different starting points. D^{max} is the maximum deviation of the cumulative graph (solid line) from the uniform distribution (dashed line). See text for detailed explanation.

veins and faults) and the amount of displacement (aperture or heave) on each of these structures. For this reason a method is needed that allows the analysis of the spatial distribution of displacements. To discuss this problem in detail, and to introduce a workflow for heterogeneity analysis, we examine two theoretical examples of brittle deformation (Fig. 1).

Fig. 1a$_1$,b$_1$ shows two examples of the same population of extensional structures that extend a layer of rock by the same amount, but with different spatial organization. The populations consist of the same three groups of structures: (i) thin veins accommodating 1.05% extension, (ii) damage zones comprising thick veins and pull-aparts that accommodate a further 3.6% extension, and (iii) faults that accommodate a further 6% extension. The damage zones always occur around the faults, but in Fig. 1a the faults and veins are uniformly distributed, whereas in Fig, 1b they are strongly clustered. The veins and faults, have heaves/apertures that obey power-law distribution (Fig. 1c); the filled circles in Fig. 1c represent the scale-range of structures shown in Fig. 1a,b.

2.3. Cumulative plots

A simple and efficient way for recording the spatial and displacement data of fracture populations is to use scan-lines (e.g. Priest, 1993), usually within a bedding plane and crossing the extensional structures perpendicular to strike. This allows extension to be measured as the one-dimensional (longitudinal), bed-parallel increase in length of a marker layer compared to its initial length by summing the bed-parallel components of fault displacements (heaves) and the bed-parallel thicknesses (apertures) of steeply-dipping veins. When using scan-lines for data collection, care has to be taken to sample the structures of interest at an appropriate resolution and over a representative distance. Based on our experience with this method we suggest that the length-scale of observation (length of the scan-line) should be at least 100 times the displacement of the largest structure examined.

The data are best presented as a plot of cumulative heave/aperture against distance (Fig. 1d), which includes the most relevant information on the spatial distribution of, and the strain accommodated by, the sampled structures. The cumulative graphs (Fig. 1d) for the two examples share common starting and ending points, and accommodate the same total strains over the observed interval. However, the total strain is distributed over a distance of about 100 m in Fig. 1a whilst it is accommodated within a zone of only 30 m in Fig. 1b. Although these are obvious and common observations when dealing with brittle deformation it is not straight forward to quantify this spatial heterogeneity of strain. To do so we introduce a measure of heterogeneity that accounts for both, the spatial

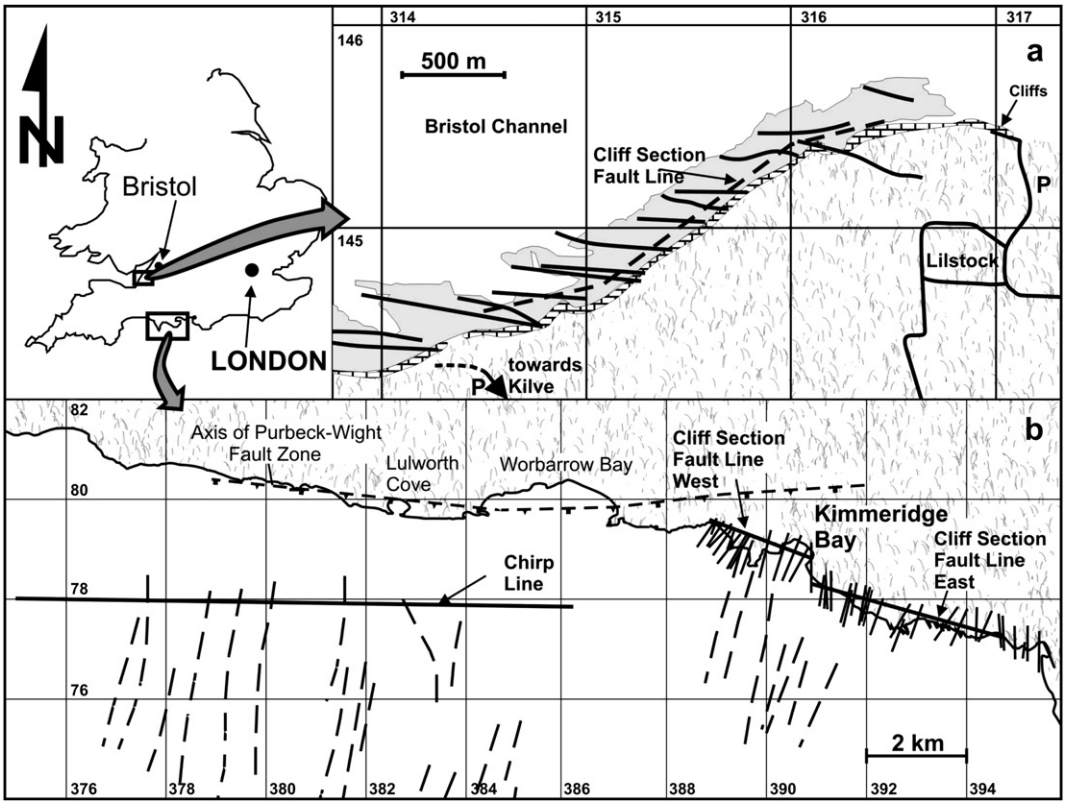

Fig. 3. Location and maps of the two study areas. (a) Coastal section with inter-tidal platforms around Kilve, Somerset; (b) coastal section around Kimmeridge Bay, Dorset. Grids and grid references refer to the British National Grid. Solid lines: major faults mapped in this study; dashed lines are fault traces as mapped by Donovan and Stride (1961). The positions of the Chirp line and the fault lines (cliff sections) are indicated.

distribution and the size (displacement) of the extensional structures.

2.4. Kuiper's method

A uniform spatial distribution of fractures or extension is represented on a cumulative plot by a straight line (Fig. 2a, dashed line). The extent to which the observed data (Fig. 2a, solid line) conform to a uniform distribution can be tested using non-parametric Kolmogorov–Smirnov tests (K–S tests). The simplest of these goodness-of-fit tests is based on the maximum deviation (D^{max}) of the observed values from the cumulative curve of the hypothesised distribution (Conover, 1980). The value of D^{max} is strongly dependent on its position (distance) on the cumulative plot as can be seen in Fig. 2a to c. For this reason, Kuiper (1960) developed a variant of the K–S test that utilises D^+ and D^-, which represent the maximum deviation above and below the proposed cumulative distribution function (Fig. 2a). Kuiper's test uses the quantity $V = |D^+| + |D^-|$ and is as sensitive in the tails as near the median of the cumulative curve. This means that the value of the test result is less dependent on the starting point of the scan-line in relation to the greatest concentration of fractures or extension.

To allow comparison of cumulative frequency and heave data over different lengths and scale ranges, the quantity V needs to be normalized by dividing by the cumulative total (T), $V' = V/T$, where T is the number of fractures or $T = \sum$(heaves) for frequency and strain analysis respectively. Fig. 2a demonstrates how V' is determined from a cumulative graph. This can either be done graphically by measuring the largest deviation above (D^+) and below (D^-) the straight-line uniform distribution or in a spread-sheet by calculating the theoretical cumulative value at each point along the scan-line and subtracting it from the observed value.

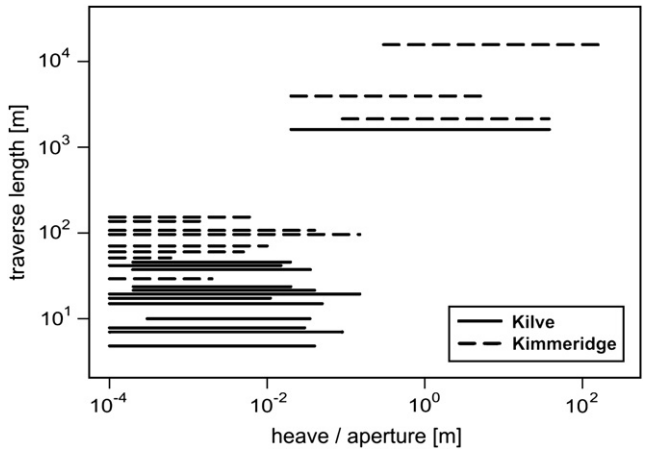

Fig. 4. Diagram showing the size-range of heaves/apertures sampled along 25 scan-lines at Kimmeridge and Kilve.

Table 1
Properties of the 25 scan-lines

Name of line	Length (m)	Bed thickness (m)	Sample size	Min. heave (m)	Max. heave (m)	Approx. position (British National Grid)
Kimmeridge						
Chirp	15700	–	153	0.33	192	E374974 N77999 – E390675 N77995
Fault E	3950	–	22	0.02	5.4	E394738 N77282 – E390938 N78350
Fault W	2150	–	16	0.09	37.76	E390948 N78862 – E388939 N79611
I-1	98	0.4	267	1.0E−04	(0.66) 0.04	E391197N78249
I-2	153	1.7–2.0	363	1.0E−04	(2.22) 0.006	E391899N77891
I-3	96	0.09–0.11	572	1.0E−04	(0.58) 0.15	E391968N77749
V-1	45	0.56	396	1.0E−04	6.00E−04	E393738 N77475
V-2	137	0.3	493	1.0E−04	1.00E−03	E392424 N77577
V-3	71	0.2	167	1.0E−04	1.00E−02	E394141 N77293
V-4	60	0.55–0.65	321	1.0E−04	4.00E−03	E399785 N76954
V-5	29	0.35	160	1.0E−04	2.00E−03	E398427 N76629
Kilve						
Fault line	1970	–	76	2.0E−03	38.1	E314510 N144490 – E316390 N145220
A1	10	0.1	10	3.0E−04	1.1E−02	E315981 N145476
A2	10	0.1	12	1.0E−03	3.5E−02	E315981 N145477
A3	7	0.1	14	1.0E−04	9.0E−02	E315981 N145478
B1B2	19	0.4	189	1.0E−04	(4) 0.15	E314747 N144510
B3	5	0.18	79	1.0E−04	4.0E−02	E314726 N144499
C1C2	42	0.3–0.6	252	1.0E−04	(25.19) 0.015	E314813N144588
D2D1	18	0.4–0.5	100	1.0E−04	(1.38) 0.011	E314934 N144631
E1	15	0.4	45	1.0E−04	5.0E−02	E315548N145181
E2	8	0.32	48	1.0E−04	3.0E−02	E315548N145182
G5G2	40	0.25	57	1.0E−04	(2.5) 0.036	E315115N144671
G6	22	0.15	53	1.0E−04	2.0E−02	E315130 N144669
G7	21	0.12	92	1.0E−04	4.0E−02	E315101 N144666
G3G1	42	0.25–0.30	60	1.0E−04	(3.7) 0.02	E315065 N144700

Coordinates refer to the British National Grid and were determined using an EGNOS-enabled hand-held GPS. Accuracies are estimated to be ±8 m. For short lines only one coordinate point is given, generally taken at the position of the largest sampled structure. Maximum heave values in parenthesises are fault-heaves of the single fault included in short lines which cross a fault zone.

To examine the spatial relationships between the larger and smaller structures (heaves/apertures) in a data-set, this procedure can be repeated several times for each scan-line with sequential removal of the largest structures from the data-set. This is particularly useful for analysis of strain heterogeneity as the largest structures cause the largest steps in cumulative heave graphs and thus may dominate the analysis. For strain-analysis the derived heterogeneities (V_S' are best plotted against the maximum heave included in each data-set to show the relationships between large and small structures (Fig. 1e). For analysis of fracture spacing the heterogeneities (V_F') are best plotted against the heave scale-range included in each data-set to display potential scale-dependencies. Throughout this paper the subscripts "S" and "F" stand for "strain" (heave/aperture) and "frequency" (number) data, respectively.

2.5. Heterogeneity at different scales

Fig. 1e shows the resulting V_S' values for the six cumulative-heave graphs (Fig. 1d) derived from the distributions shown in Fig. 1a,b. To examine the strain-heterogeneity at different scales the largest structures were removed from both data-sets in half-order-of-magnitude steps and V_S' determined for each step to analyse the scale-dependency of strain-heterogeneity in the two examples (Fig. 1e). The corresponding sketches (with the largest structures removed) are shown in Figs. 1a_2,a_3 and b_2,b_3.

Comparison of the two complete data-sets shows that the spatial heterogeneity in a_1 ($V_S' = 0.42$) is lower than in b_1 ($V_S' = 0.75$). Sequential removal of the largest structures rapidly reduces the value of V_S' in case a, but has only a minor effect in case b (Fig. 1e). Thus, small-scale extension in case a_3 is homogenously distributed ($V_S' = 0.02$) whilst in case b_3 it is heterogeneous ($V_S' = 0.70$). In case a, the strain is moderately heterogeneous at the fault-scale ($V' = 0.42$), but homogeneous for the thin veins ($V_S' = 0.02$), and is hence scale-dependent. Whereas the strain-heterogeneity in case b is scale-invariant, being high over the entire observed scale-range ($0.7 \leq V' \leq 0.75$).

2.6. Statistical significance of the derived heterogeneities

Having described the workflow for heterogeneity-analysis based on Kuiper's Test using theoretical examples (Fig. 1), we are now in a position to apply the method to real data-sets. Before doing this however, we should seek to establish if the determined heterogeneities are statistically significant. This can be done by determining whether the heterogeneity (V') is significantly different from a uniform distribution given the sample size (n). To do this, Stephens (1965) proposed a parameter $V^* = n^{1/2} \times V'$ for Kuiper's test, and tabulated critical

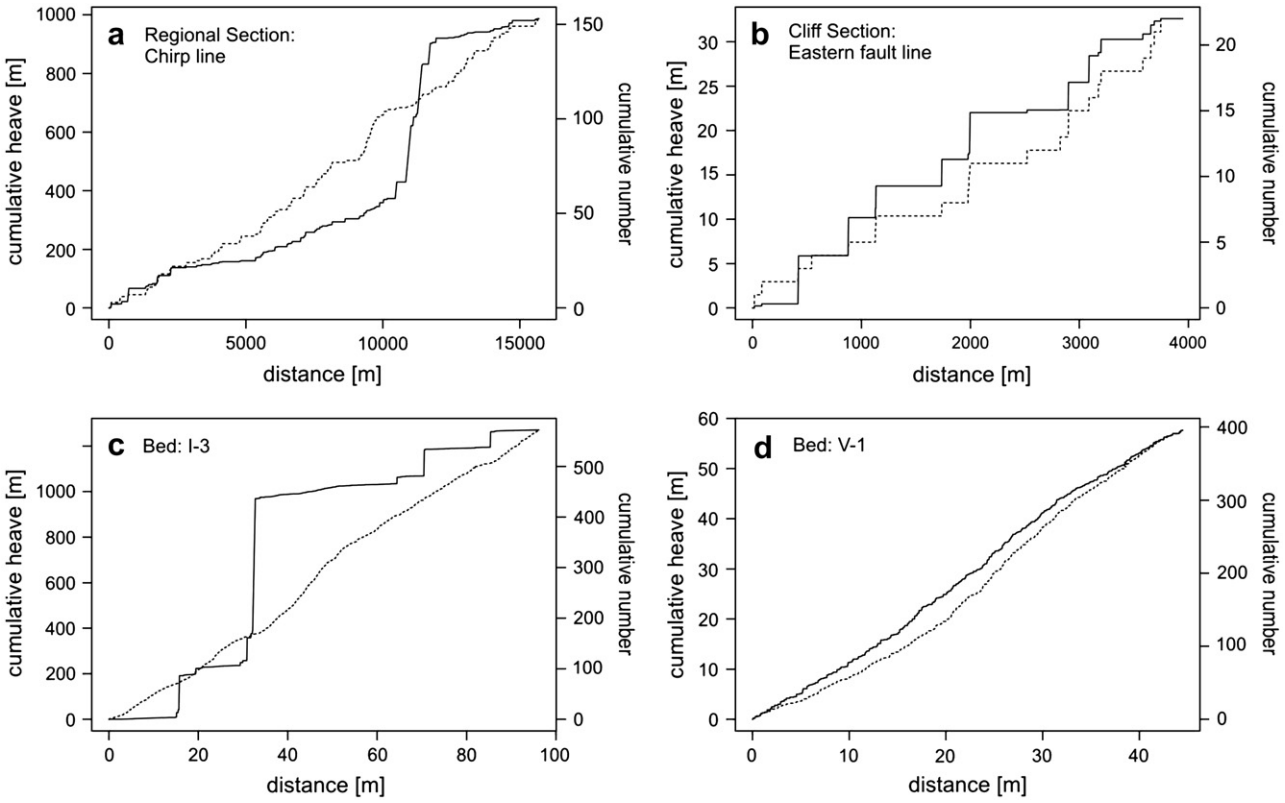

Fig. 5. Selected cumulative heave/aperture (solid lines) and number (dashed lines) plots from Kimmeridge. (a) High resolution seismic section (Chirp line) with 154 faults. (b) Cliff section (Eastern fault line) with 22 faults. (c) Short section (96 m) tracing a single carbonate bed across a fault with 0.6 m heave sampling 572 fractures. (d) Short section (45 m) tracing a single carbonate bed far away (>50 m) from the closest fault sampling 396 veins.

values for rejection of the null hypothesis of the uniform distribution (see also Mardia, 1972). For large n, say >50, the critical value is $V^* \approx 1.7$ at the 0.05 (5%) level. Data-sets that are not significantly different from a uniform distribution are either homogeneous or have too small a sample-size to allow rejection of this hypothesis. Applying this test to the example cases from Fig. 1 confirms that all data-sets are significantly different from a uniform distribution apart from a_3 which conforms to a uniform distribution.

3. Application: field studies

3.1. Geological overview

Two study areas in southern England (Fig. 3) were chosen as they provide cliff sections of continuous exposure that are several kilometres long. In both areas, sets of normal faults and tensile fractures, formed during a single tectonic event, are exposed and intersected by the cliffs at high angles. The size, position and orientation of the extensional structures were collected in 25 lines of different length and resolution (Fig. 4 and Table 1). At Kilve, 14 scan-lines sample structures with a total displacement range of more than 5 orders of magnitude. At Kimmeridge Bay, 10 scan-lines cover a similar displacement scale-range that is extended to more than 6 orders of magnitude by an additional high-resolution seismic line (Chirp) running about parallel to the coast line (Hunsdale et al., 1998).

The sedimentary sequence exposed in the cliffs and intertidal platforms around Kilve consists of Triassic marls and Jurassic limestones, shales and marls (Whittaker and Green, 1983). Palmer (1972) divided the sequence based on lithological differences. Most prominent is the limestone/shale interbedded Blue Lias in the studied sequence, above and below which are the mudstone dominated units of the St. Audrie's and Kilve Shales, respectively. The shale/carbonate ratio of the examined section is about 5/1.

The type section of the Upper Jurassic Kimmeridge Clay at Kimmeridge Bay consists mainly of mudrocks with some intercalated white coccolithic limestones and minor grey and yellow limestones and dolostones (Morgans-Bell et al., 2001). The shale/carbonate ratio of the exposed section is about 13/1.

Numerous carbonate beds within both stratigraphic successions provide useful marker-beds that can be traced and correlated across each study area. The high stratigraphic resolution (≤0.2 m) of the well-studied sedimentary sequences (Whittaker and Green, 1983; Morgans-Bell et al., 2001) allows displacement to be accurately determined on faults over a wide range of scales. Fault-displacements of up to 5 m can be directly measured in the cliffs and larger displacements can be inferred using stratigraphic separation across faults and fault orientation measurements. Associated veins

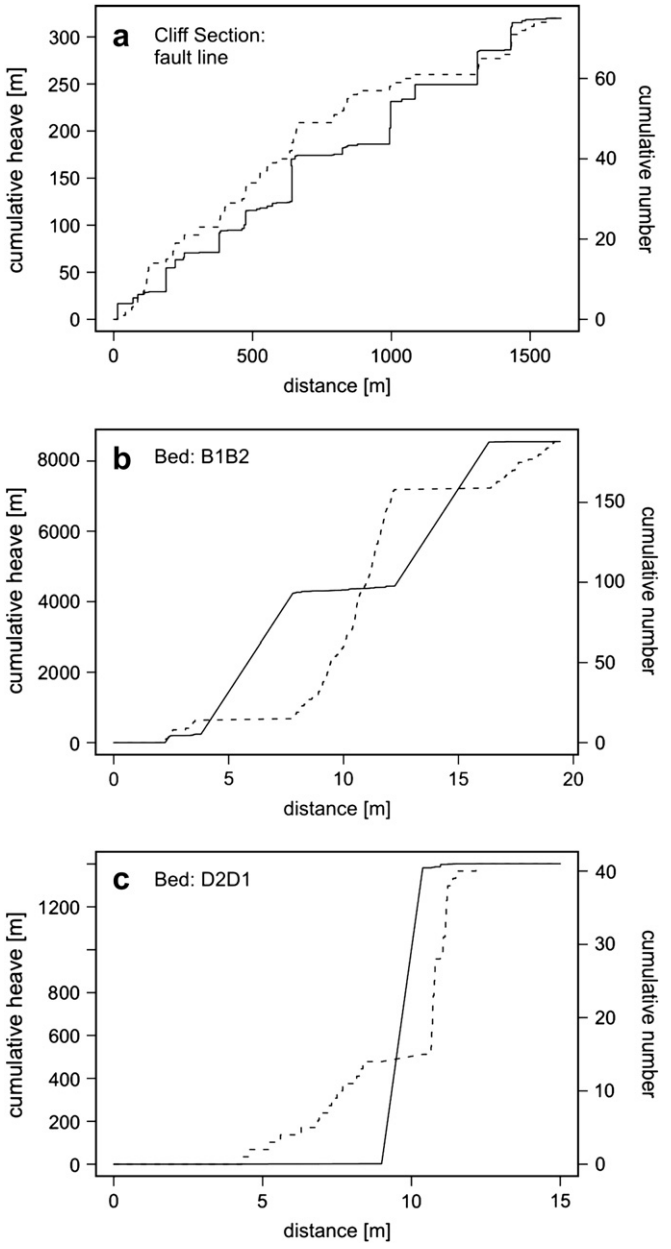

Fig. 6. Selected cumulative heave/aperture (solid lines) and number (dashed lines) plots from Kilve. (a) Cliff section (1.97 km) with 76 faults. (b) Short section (19 m) tracing a carbonate bed across 2 faults with heaves of about 4 m and sampling 189 fractures. (c) Short section (18 m) tracing a carbonate bed across a fault with 1.4 m heave and sampling 100 fractures.

have openings that can be measured to <1 mm in the carbonate marker-beds.

Both study areas lie within a large extensional region – the Wessex Basin. This region underwent north–south extension from Permian to mid-Cretaceous times, leading to the development of a series of normal faults (Chadwick, 1985; Karner et al., 1987; Lake and Karner, 1987; Underhill and Stoneley, 1998). Major basin-bounding and intra-basinal faults strike east-west and most major faults dip to the south. Active crustal extension ceased in the Aptian, and the region underwent widespread thermal subsidence (Chadwick, 1993).

In the lower Tertiary, there is evidence for a change of structural style in the Wessex Basin. Many east-west striking normal faults were reactivated or inverted in response to north-south compression (Chadwick, 1993; Dart et al., 1995). During Oligocene–Miocene times, the north–south compression led to the development of conjugate strike-slip faults in some areas (e.g. North Somerset, Peacock and Sanderson, 1998; Lyme Bay, Harvey and Stewart, 1998) and to conjugate, north–south striking extensional faults in the Weymouth Bay region (Hunsdale and Sanderson, 1998).

Thus the sections studied at Kilve and Kimmeridge represent different tectonic events. Those at Kilve (Fig. 3a) are dominated by the early extensional event (pre-Aptian) and none of the faults show evidence of later inversion (Peacock and Sanderson, 1998). The normal faults and veins around Kimmeridge Bay (Fig. 3b) were produced during the late extensional event associated with the inversion phase (Hunsdale and Sanderson, 1998).

3.2. Data

Extension is measured as the one-dimensional (longitudinal), bed-parallel increase in length of a marker-bed compared to its initial length. As the beds in both study areas are flat-lying, the extension accommodated by discrete structures is easily quantified by summing the bed-parallel components of fault displacements (heaves) and the bed-parallel thicknesses (apertures) of steeply-dipping veins. To do this in a consistent manner, over the entire scale-range and across different structures, data were collected along straight lines oriented at high angles to the regional trend of the faults. For each fracture encountered along a traverse, its distance from the origin of the line, its heave (for faults) or thickness (for veins), and its dip and strike were measured. Errors due to oblique sampling were corrected for by applying the methods described by Terzaghi (1965) and Peacock and Sanderson (1993). Locations and physical characteristics of all 25 data-sets are summarised in Table 1 and their heave/aperture-ranges and lengths compared in Fig. 4. The 4 fault-lines (Seismic line and cliff sections) sample the fault-strain whilst the 21 shorter scan-lines cover zones of intense damage surrounding faults and low-damage host-rock in between fault zones. Seven representative cumulative heave and number plots from the two study areas are shown in Figs. 5 and 6.

4. Interpretation

Heterogeneity analysis based on the cumulative distribution was carried out for all 25 field data-sets as described in the previous sections. The method was applied to both the cumulative number (fracture frequency) and the cumulative heave (extension) data and the statistical significance of the determined heterogeneities tested using Kuiper's test. Values of the heterogeneity measure (V') for fracture frequency (V_F') and strain (V_S') for all data-sets are listed in Table 2 together with the coefficient of variation (C_V) that was determined for fracture spacing in each data-set.

Table 2
Summary of statistical data of the 25 data-sets

Name of line	Fract. spac (m)	Extension (%)	V_F'	V_F*	Stat. sign. of V_F	C_V*	V_S'	V_S*	Stat. sign. of V_S
Kimmeridge									
Chirp	102.6	6.7	0.123	1.53	n.s.	1.4	0.459	5.68	***
Fault E	179.5	0.8	0.194	0.91	n.s.	1.02	0.261	1.22	n.s.
Fault W	134.0	4.3	0.185	0.74	n.s.	0.74	0.411	1.84	*
I-1	0.33	0.43	0.119	1.94	*	0.82	0.464	11.29	***
I-2	0.40	0.05	0.116	3.15	***	0.84	0.46	11.97	***
I-3	0.17	0.73	0.101	2.41	***	0.71	0.373	13.68	***
V-1	0.11	0.13	0.131	2.6	***	0.88	0.096	1.91	**
V-2	0.26	0.07	0.171	3.8	***	0.82	0.136	2.42	***
V-3	0.42	0.08	0.203	2.62	***	1.01	0.311	4.02	***
V-4	0.19	0.23	0.07	1.25	n.s.	0.81	0.086	1.53	n.s.
V-5	0.18	0.24	0.102	1.29	n.s.	0.79	0.172	2.18	***
Kilve									
Fault line	25.9	24.75	0.244	2.11	***	1.65	0.14	1.21	n.s.
A1	1.00	0.23	0.881	2.79	***	2.55	0.937	2.81	***
A2	0.83	1.01	0.682	2.36	***	1.77	0.776	2.57	***
A3	0.50	1.78	0.634	2.37	***	1.91	0.919	3.31	***
B1B2	0.10	2.32	0.536	7.37	***	2.64	0.476	6.49	***
B3	0.06	3.76	0.464	4.12	***	1.43	0.571	5.04	***
C1C2	0.17	0.51	0.602	9.56	***	9.61	0.605	9.57	***
D2D1	0.18	0.20	0.437	4.37	***	3.24	0.533	5.27	***
E1	0.33	2.13	0.668	4.48	***	4.54	0.731	4.85	***
E2	0.17	2.00	0.372	2.58	***	1.84	0.501	3.33	***
G5G2	0.70	0.31	0.637	4.81	***	5.05	0.672	4.99	***
G6	0.42	0.54	0.721	5.25	***	5.4	0.731	5.27	***
G7	0.23	1.67	0.434	4.16	***	3.67	0.663	6.32	***
G3G1	0.70	0.26	0.629	4.83	***	6.3	0.466	3.58	***

The second column lists the average fractures spacing for each line. The third column gives the bulk extensional strain measured on each transect. Columns 4 to 10 list the results of the heterogeneity analysis for fracture spacing (C_V* and V_F') and strain distribution (V_S'). The asterisks indicate the statistical significance of the determined deviations from uniform distribution at probabilities of 0.005 (***), 0.01 (**) and 0.05 (*) respectively; n.s., not significant. C_V* is the modified coefficient of variation of fracture spacing. V_F' and V_S' are the test results of Kuiper's test for the heterogeneity of fracture spacing and strain, respectively.

In Fig. 7a and b the determined values of V_F' and V_S' are plotted against sample-size; the three curves in the diagrams represent the critical values for rejection of the null hypothesis of the uniform distribution at confidence levels of 90%, 95% and 99.5% respectively (Stephens, 1965).

Fig. 7a shows that fractures in all data-sets from Kilve are significantly different from a uniform distribution, whilst most of the data from Kimmeridge are only weakly heterogeneous and for some of these a uniform distribution of fractures cannot be ruled out. Fig. 7b shows that extension in all but one data-set from Kilve is significantly heterogeneous. At Kimmeridge strain is significantly heterogeneous in most of the data although some data-sets show only weak heterogeneity and for two a uniform distribution of extension cannot be ruled out.

The cross-plot of the heterogeneity measures for fracture frequency (V_F') and extension (V_S') (Fig. 7c) emphasises this difference. The data from Kilve show a strong correlation between fracture-clustering and heterogeneity of extension, whilst the data from Kimmeridge show very low heterogeneity of fracture-distribution, independent of the heterogeneity of extension. Fig. 7d,e shows the dependence of the heterogeneity measures (V') from the bulk-extension recorded for each line-sample. It can be seen that both, the heterogeneities of fracture distribution and of extension, are higher at Kilve than at Kimmeridge up to extensions of about 10%. At higher extensions the heterogeneity goes down implying uniform fracture and strain distributions. These relationships are discussed in detail in the following section.

4.1. Scale dependency of fracture clustering

Fig. 8a shows the derived heterogeneities (V_F') with respect to the structure-size range sampled in each data-set (min. heave–max. heave). It can be seen that at a heave scale-range between 10^{-4} m and 10^{-2} m (thin veins) the data from the two study areas form two distinct clusters. The Kilve data show moderate to high spatial heterogeneity ($0.37 \leq V_F' \leq 0.88$) whilst those from Kimmeridge are more homogeneous ($0.07 \leq V_F' \leq 0.20$). At the fault-scale (10^{-1}–10^{2} m heave) the heterogeneity in the Kilve data are still somewhat higher ($V_F' = 0.24$) than at Kimmeridge ($0.12 \leq V_F' \leq 0.19$), but the low values indicate only weak heterogeneity of fault-spacing in both regions.

Determination of the coefficient of variation (C_V) for fracture spacing supports the above observations and allows discrimination between regular and random distributions of fractures, both of which show low spatial heterogeneity and thus yield low values of V_F'. Fig. 8c shows the derived C_V* values with respect to the structure-size range sampled in each data-set (min. heave–max. heave). At the lower end of

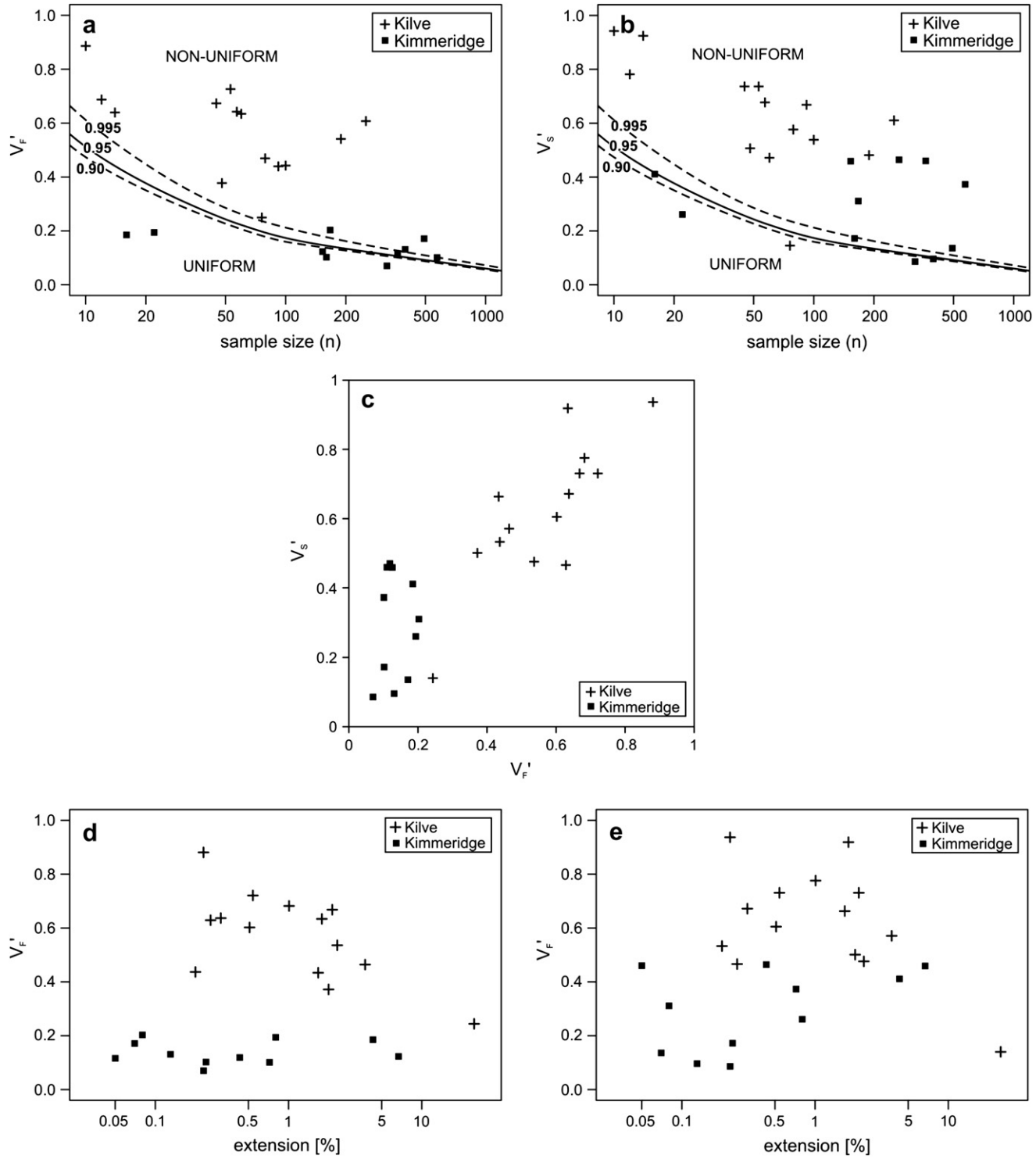

Fig. 7. (a) and (b) are plots of the heterogeneity measures (V') with respect to the sample size n. (a) heterogeneity of fracture frequency (V_F') and (b) heterogeneity of strain distribution (V_S'). The three curves labelled 0.995, 0.95 and 0.90 are the critical values for Kuiper's test (Stephens, 1965) for the probabilities with 90%, 95% and 99.5% confidence that a data-set is significantly different from a uniform distribution. Values below the lines are not significantly heterogeneous whilst values above the curves are significantly heterogeneous. (c) is a cross-plot of V_S' against V_F'. (d) and (e) are plots of the heterogeneity measures (V') with respect to the extension recorded for each line-sample. (d) heterogeneity of fracture frequency (V_F') and (b) heterogeneity of strain distribution (V_S').

the scale range (10^{-4}–10^{-2} m heave) the Kilve data show significantly clustered veining ($1.4 \leq C_V^* \leq 5.40$) compared to random or slightly anti-clustered distributions of veins at this scale-range in the Kimmeridge data-sets ($0.71 \leq C_V^* \leq 1.01$). The spacings of faults with 10^{-1}–10^{2} m heave in both regions are close to random distributions with the Kilve data showing somewhat more clustering ($C_V^* = 1.65$) than the Kimmeridge data ($0.74 \leq C_V^* \leq 1.4$).

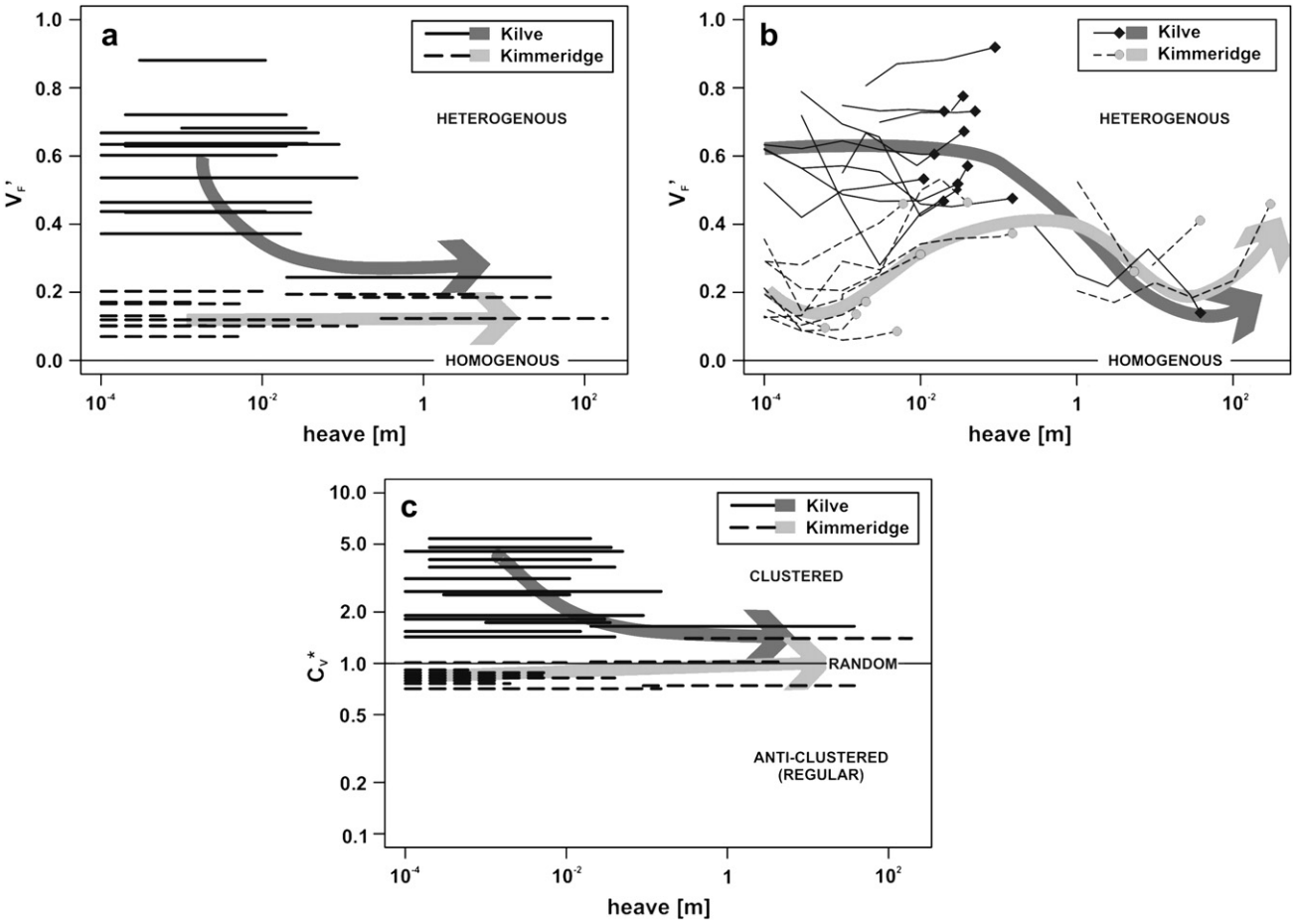

Fig. 8. Plots of heterogeneity measures (V') for the 25 scan-lines. (a) Frequency-heterogeneity (V_F') versus heave-range. (b) Strain-heterogeneity (V_S') for complete data-sets is represented by filled diamonds and circles. Heterogeneities after removal of the largest structures in half-order-of-magnitude steps are shown as tails to the left of each complete data-set. (c) Coefficient of variation (C_V*) versus heave-range for fracture-spacing.

To summarise these results, it can be said that the fracture population sampled at Kimmeridge shows no scale-dependence of fracture distribution and that the fractures show random or only weakly heterogeneous distributions over the entire sampled scale-range. At Kilve, on the other hand, the heterogeneity of fracture-spacing shows a strong scale-dependence with veins being highly clustered around normal faults which themselves display only weak heterogeneity in their spatial distribution.

4.2. Scale-dependency of strain heterogeneity

In Fig. 8b, V_S' values for all scan-lines are plotted against the maximum heave included in each data-set. Diamonds and circles represent the heterogeneity of the complete data-set, whilst the tails to the left show the heterogeneity of the data after removal of the largest structures in half-order-of-magnitude steps. It can be seen that V_S' is strongly scale-dependent for all data-sets as indicated by the arrows that give the general trends of heterogeneity for the two study areas (Fig. 8b).

At the lower end of the scale range (10^{-4}–10^{-2} m aperture) there is a clear separation between the data from the two study areas. Strain accommodated by veins at Kimmeridge is almost uniformly distributed ($V_S' < 0.2$) whilst similar data from Kilve show high heterogeneity ($V_S' \geq 0.5$) indicating localized strain.

At the scale-range of 10^{-2}– 10^{0} m heave, the heterogeneities in the two study areas are converging (Fig. 8b), but the Kilve data still show higher heterogeneity ($0.45 \leq V_S' \leq 0.9$) than the Kimmeridge data ($0.3 \leq V_S' \leq 0.5$). The structures dominating this scale-range are thick veins and pull-aparts (Fig. 9d) (Peacock and Sanderson, 1995) and are confined to damage zones adjacent to faults in both study-areas.

At the fault-scale (10^{0}–10^{2} m heave) the two study areas show a very similar signature in terms of strain distribution. Fault-strain is only weakly heterogeneous ($0.1 < V_S' \leq 0.4$) in both study-areas with only somewhat higher heterogeneity at Kimmeridge than at Kilve. At the high end of the sampled scale-range there is some suggestion that heterogeneity increases ($V_S' > 0.4$) for the larger faults (>100 m heave), which may indicate localisation of strain onto these faults.

4.3. Evolution of extensional strain in the two study areas

Fig. 10 compares the observed structures for different stages of extension in the two study areas. At Kimmeridge

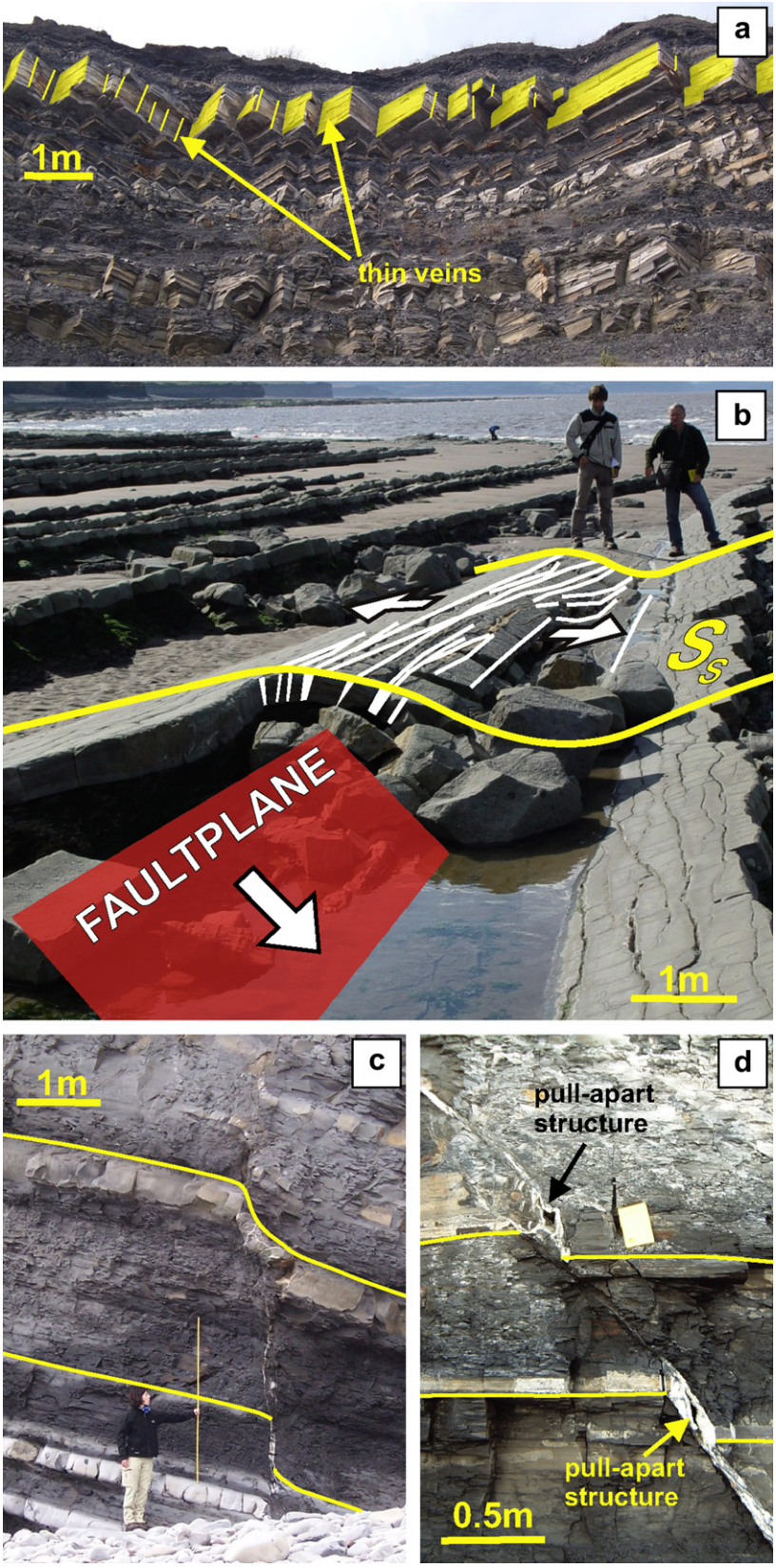

Fig. 9. Photographs of typical structures observed in the two study areas. (a) The set of highlighted surfaces and lines are thin, parallel veins with regular spacing in a carbonate bed at Kimmeridge (compare to Fig. 10a_1). (b) ''Blind fault'' at Kilve. The hidden fault plane with slip direction is indicated. S_S is the bedding surface which is bent and intensely veined due to process zone damage close to the upper tip of the indicated fault. Tensile veins are highlighted (compare to Fig. 10b_1). (c) Break through of a normal fault after bending of carbonate beds in the process zone close to the upper tip of a normal fault at Kilve (compare to Fig. 10b_3). (d) Pull-apart structures developed in carbonate beds at Kimmeridge (compare to Fig. 10a_2).

(Fig. 10a) early extension is accommodated by distributed tensile failure of the carbonate beds throughout the entire region (Fig. 9a) whilst the shales appear to accommodate deformation by shear failure on many planes (Fig. 10a_1) (Putz and Sanderson, in press). These early thin veins show regular spacing and no increase in frequency towards faults which indicates that these they not formed synchronously with faulting (Peacock, 2001). In some rotated blocks within fault-zones the thin veins are preserved, supporting the interpretation that they pre-date the faulting. Increased extension localises displacement onto a few regularly spaced shear planes and opens veins to form pull-apart structures and minor faults (Figs. 10a_2 and 9d). These structures occur only in damage zones around faults, and are thus interpreted to be caused by localisation of strain prior, and during faulting. Finally some fault planes break through and further increase in strain is accommodated dominantly by slip on these planes (Fig. 10a_3).

At Kilve (Fig. 10b) early extension is highly localised in narrow zones (typically 1–5 m wide) preserving large proportions of virtually undeformed rocks in between (Fig. 10b_1). Tensile deformation around the tip zones of propagating faults (process-zone) seems to be the dominant deformation mechanism in the carbonate beds (Fig. 9b) (Schöpfer et al., 2006). Small displacements are accommodated by bending of the carbonate beds and opening (thickening) of veins (Fig. 10b_2) until the fault breaks through to facilitate slip (Figs. 9c and 10b_3). Once a network of faults is formed further increase in strain is accommodated dominantly by slip on the fault system.

A tentative hypothesis for the different early-extensional behaviour in the two study areas may lie in their lithological differences. Both areas examined consist of interbedded mudstones and carbonates, but in very different proportions. The Kimmeridge Clay is dominated by shales (shale:carbonate $\approx$13:1), with only a few 0.1–0.5 m thick limestones. These are useful marker beds but probably have little influence on

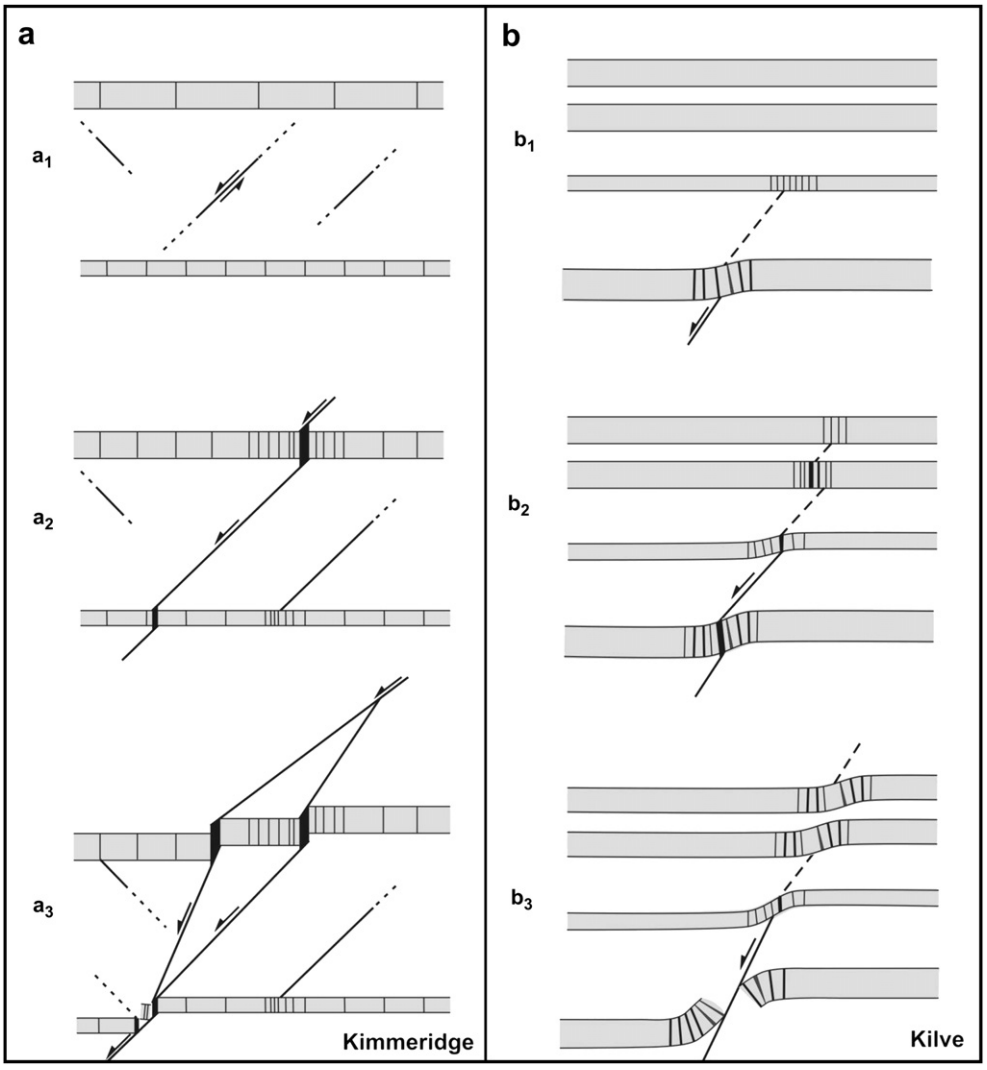

Fig. 10. Conceptual models of the early-stage evolution of extension-related damage in the mudstone-dominated and in the more carbonate-rich sequence at Kimmeridge (a) and Kilve (b) respectively. The sketches show the evolution from low strain (a_1 and b_1) to higher strain values (a_3 and b_3).

the overall strength and stiffness of the sequence. The rocks exposed around Kilve, on the other hand, comprise an interlayered sequence of shales and carbonates (in the ratio ≈5:1), in which the carbonates may substantially increase the mechanical strength and stiffness of the rocks. Further study is necessary to test this hypothesis.

5. Discussion and conclusions

A method for spatial analysis of cumulative data has been presented and applied to spacing and displacement data from two extensional regions in the southern UK. This method yields both a measure of the heterogeneity of the distribution of fracture frequency and strain, and a statistic (based on Kuiper's test) that may be used to test for significant departures from a uniform distribution. The results of this study allow us to address the three questions raised in the introduction and answer them for the two studied regions:

5.1. How is extensional brittle strain distributed in a volume of rock?

Twenty-five data-sets of different lengths (7–15,700 m) and displacement-resolution (0.1 mm–0.5 m lower limit) from two study areas in the Southern UK have been analysed in terms of their strain-distribution over a total displacement scale-range of about 6 orders of magnitude (10^{-4}–10^{2} m). Fault-strain in both regions is found to be weakly heterogeneous ($0.1 < V_S' < 0.5$) at a fault-heave range from 10^{0}–10^{2} m. In the scale range 10^{-2}–10^{0} m, thick veins and pull-apart structures are localized in damage zones adjacent to faults and thus show a high spatial heterogeneity in both regions ($0.4 < V_S' < 0.9$). The most significant differences in strain-heterogeneity between the two study areas were found at the scale-range of small tensile fractures (10^{-4}–10^{-2} m). These fractures (veins) are clustered and thus the strain on them is localized within narrow damage zones around faults in the more carbonate-rich sequences at Kilve ($0.5 < V_S' < 0.8$), whilst they are almost uniformly distributed across the entire region in the mudstone-dominated sequence at Kimmeridge ($V_S' < 0.2$).

5.2. What are the spatial relationships between faults and veins formed during the same event?

The majority of small, tensile fractures were found to have formed during the early-stage extension in both study areas. However, the spatial distribution of these early fractures is significantly different in the two regions. At Kimmeridge they accommodate a fairly uniform ($V_S' < 0.2$) ''background strain'' distributed across the entire region on randomly spaced fractures, whilst they are highly clustered and accommodate a localized strain at Kilve ($V_S' \sim 0.5$). This implies that the majority of tensile fractures at Kimmeridge formed independently of and predate the normal faults in the region. At Kilve most of the small-scale damage is related to the tips of propagating normal faults (Kim et al., 2003; Schöpfer et al., 2006) and thus is found only within narrow zones adjacent to these faults.

Faults in both regions are fairly uniformly (randomly) distributed ($0.74 \leq Cv^* \leq 1.65$) and are associated with pull-apart structures and thick veins that developed as slip accumulated. At Kilve this kinematic damage is superimposed on the earlier tip-damage (process zone); together these define relative narrow (0–5 m wide) damage zones adjacent to faults, leaving zones of virtually undeformed host-rock in between fault-zones. At Kimmeridge the kinematic-damage zones surrounding faults are much wider (20– 60 m) and are separated from adjacent damage-zones by background-vein zones.

Consequently it can be said that the spatial heterogeneity of fractures and strain sampled at Kimmeridge show virtually no scale-dependence, whilst similar data from Kilve are strongly scale-dependent.

5.3. How do fracture populations evolve with increasing strain?

A general trend could be described as follows: the more carbonate-rich sequence (Kilve) deforms by discrete faulting and tends to localize deformation at an early stage. The mudstone-dominated sequence (Kimmeridge) accommodates initial deformation in a more distributed manner. Once through-going faults are formed both sequences deform in a similar manner by accumulating slip on the larger faults. A result of these different early-stage deformation-styles is that mudstone dominated sequences display low spatial heterogeneity of small scale deformation (veining) whilst more carbonate-rich sequences show clustered veining and thus significant spatial heterogeneity. It is also worth mentioning that the majority of small-scale structures in both study areas formed during early-stage extension and did not change notably during later strain localisation onto the fault system.

Acknowledgements

Martin Putz gratefully acknowledges a Janet Watson PhD Scholarship from Imperial College London and a Central Research Fund Grant 2006/07 from the University of London. Ulrike Freitag is thanked for help with some of the field work. The positive reviews by C. Childs and G. Yielding were greatly appreciated.

References

Ackermann, R.V., Schlische, R.W., Withjack, M.O., 2001. The geometric and statistical evolution of normal fault systems: an experimental study of the effects of mechanical layer thickness on scaling laws. Journal of Structural Geology 23, 1803–1819.

Antonellini, M., Aydin, A., 1995. Effect of faulting on fluid flow in porous sandstones; geometry and spatial distribution. AAPG Bulletin 79, 642–671.

Bailey, W.R., Walsh, J.J., Manzocchi, T., 2005. Fault populations, strain distribution and basement fault reactivation in the East Pennines Coalfield, UK. Journal of Structural Geology 27, 913–928.

Belayneh, M., Masihi, M., Matthäi, S.K., King, P.R., 2006. Prediction of vein connectivity using the percolation approach: model test with field data. Journal of Geophysics and Engineering 3, 219–229.

Billi, A., Salvini, F., Storti, F., 2003. The damage zone-fault core transition in carbonate rocks: implications for fault growth, structure and permeability. Journal of Structural Geology 25, 1779–1794.

Bonnet, E., Bour, O., Odling, N.E., Davy, P., Main, I., Cowie, P., Berkowitz, B., 2001. Scaling of fracture systems in geological media. Reviews of Geophysics 39, 347–383.

Caine, J.S., Evans, J.P., Forster, C.B., 1996. Fault zone architecture and permeability structure. Geology 24, 1025–1028.

Chadwick, R.A., 1985. Permian, Mesozoic and Cenozoic structural evolution of England and Wales in relation to the principles of extension and inversion tectonics. In: Whittaker, A. (Ed.), Atlas of Onshore Sedimentary Basins in England and Wales: Post Carboniferous Tectonics Stratigraphy. Blackie, New York, pp. 9–25.

Chadwick, R.A., 1993. Aspects of basin inversion in southern Britain. Journal of the Geological Society London 150, 311–322.

Conover, W.J., 1980. Practical nonparametric statistics. John Wiley & Sons, New York.

Crampin, S., 1994. The fracture criticality of crustal rocks. Geophysics Journal International 118, 428–438.

Dart, C.J., McClay, K., Hollings, P.N., 1995. 3D analysis of inverted extensional fault systems, southern Bristol Channel basin, U.K. In: Buchanan, J.G.B.P.G. (Ed.), Basin Inversion, vol. 88. Geological Society, London, pp. 393–413. Special Publications.

Dawers, N.H., Anders, M.H., Scholz, C.H., 1993. Growth of normal faults: displacement-length scaling. Geology 21, 1107–1110.

Donovan, D.T., Stride, A.H., 1961. An acoustic survey of the sea floor south of Dorset and its geological interpretation. Philosophical Transactions of the Royal Society of London 44, 299–330.

Evans, J.P., Forster, C.B., Goddard, J.V., 1997. Permeability of fault-related rocks, and implications for hydraulic structure of fault zones. Journal of Structural Geology 19, 1393–1404.

Gillespie, P.A., Howard, C.B., Walsh, J.J., Watterson, J., 1993. Measurement and characterisation of spatial distributions of fractures. Tectonophysics 226, 113–141.

Gillespie, P.A., Walsh, J.J., Watterson, J., Bonson, C.G., Manzocchi, T., 2001. Scaling relationships of joint and vein arrays from The Burren, Co. Clare, Ireland. Journal of Structural Geology 23, 183–201.

Gillespie, P., 2003. Comment on ''The geometric and statistical evolution of normal fault systems: an experimental study of the effects of mechanical layer thickness on scaling laws'' by Ackermann, R.V., Schlische, R.W., Withjack, M.O. Journal of Structural Geology 25, 819–822.

Gross, M.R., Engelder, T., 1995. Strain accommodated by brittle failure in adjacent units of the Monterey Formation, USA: scale effects and evidence for uniform displacement boundary conditions. Journal of Structural Geology 17, 1303–1318.

Gupta, A., Scholz, C.H., 2000. Brittle strain regime transition in the Afar depression: implications for fault growth and seafloor spreading. Geology 28, 1087–1090.

Harvey, M.J., Stewart, S.A., 1998. In: Underhill, J.R. (Ed.), Development, Evolution and Petroleum Geology of the Wessex Basin. Influence of salt on the structural evolution of the Channel Basin, vol. 133. Geological Society, London, pp. 241–266. Special Publications.

Hunsdale, R., Sanderson, D.J., 1998. Fault distribution analysis, an example from Kimmeridge Bay, Dorset, U.K. In: Underhill, J.R. (Ed.), Development, Evolution and Petroleum Geology of the Wessex Basin, vol. 133 Geological Society, London, pp. 299–310. Special Publications.

Hunsdale, R., Bull, J.M., Dix, J.K., Sanderson, D.J., 1998. The use of high-resolution seismic reflection profiles for fault analysis in the near-shore environment, Weymouth Bay, Dorset, England, United Kingdom. Journal of Geophysical Research 103, 15409–15422.

Jourde, H., Flodin, E.A., Aydin, A., Durlofsky, L.J., Wen, X.H., 2002. Computing permeability of fault zones in eolian sandstone from outcrop measurements. AAPG Bulletin 86, 1187–1200.

Kachanov, M., 1992. Effective elastic properties of cracked solids: critical review of some basic concepts. Applied Mechanics Review 45, 304–335.

Karner, G.D., Lake, S.D., Dewey, J.F., 1987. In: Hancock, J.F., Dewey, J.F., Coward, M.P. (Eds.), Continental Extension Tectonics. The thermo-mechanical development of the Wessex Basin, southern England, vol. 28. Geological Society, London, pp. 517–536. Special Publications.

Kim, Y.-S., Peacock, D.C.P., Sanderson, D.J., 2003. Mesoscale strike-slip faults and damage zones at Marsalforn, Gozo Island, Malta. Journal of Structural Geology 25, 793–812.

Kuiper, N.H., 1960. Tests concerning random points on a circle. Nederlandes Akademie van Wetenschappen Proceedings A36, 38–47.

Lake, S.D., Karner, G.D., 1987. The structure and evolution of the Wessex Basin, southern England: an example of inversion tectonics. Tectonophysics 137, 347–378.

Mardia, K.V., 1972. Statistics of Directional Data. Academic Press Inc., London Ltd.

Marrett, R., Allmendinger, R.W., 1991. Estimates of strain due to brittle faulting: sampling of fault populations. Journal of Structural Geology 13, 735–738.

Marrett, R., Allmendinger, R.W., 1992. Amount of extension on ''small'' faults: an example from the Viking graben. Geology 20, 47–50.

Matthäi, S.K., Aydin, A., Pollard, D.D., Roberts, S., 1998. Numerical simulation of deviations from radial drawdown in a faulted sandstone reservoir with joints and zones of deformation bands. In: Jones, G., Fisher, Q.J., Knott, S.D. (Eds.), Faulting, fault sealing and fluid flow in hydrocarbon reservoirs, vol. 147. Geological Society, London, pp. 157–191. Special Publications.

Morgans-Bell, H.S., Coe, A.L., Hesselbo, S.P., Jenkyns, H.C., Weedon, G.P., Marshalls, J.E., Tyson, R.V., Williams, C.J., 2001. Integrated stratigraphy of the Kimmeridge Clay Formation (Upper Jurassic) based on exposures and boreholes in south Dorset, UK. Geological Magazine 138, 511–539.

Palmer, C.P., 1972. The Lower Lias (Lower Jurassic) between Watchet and Lilstock in North Somerset (United Kingdom). Newsletters on Stratigraphy 2, 1–30.

Peacock, D.C.P., 2001. The temporal relationship between joints and faults. Journal of Structural Geology 23, 329–341.

Peacock, D.C.P., Sanderson, D.J., 1993. Estimating strain from fault slip using a line sample. Journal of Structural Geology 15, 1513–1516.

Peacock, D.C.P., Sanderson, D.J., 1994. Strain and scaling of faults in the chalk at Flamborough Head, U.K. Journal of Structural Geology 16, 97–107.

Peacock, D.C.P., Sanderson, D.J., 1995. Pull-aparts, shear fractures and pressure solution. Tectonophysics 241, 1–13.

Peacock, D.C.P., Sanderson, D.J., 1998. Deformation history and basin-controlling faults in the Mesozoic sedimentary rocks of the Somerset coast. Proceedings Geologist's Association 110, 41–52.

Pickering, G., Bull, J.M., Sanderson, D.J., 1996. Scaling of fault displacements and implications for the estimation of sub-seismic strain, vol. 99. Geological Society, London. Special Publications, 11-26.

Priest, S.D., 1993. Discontinuity analysis for rock engineering. Chapman & Hall, London.

Putz, M.W., Sanderson, D.J., in press. The distribution of faults and fractures and their importance in accommodating extensional strain at Kimmeridge Bay, Dorset, UK, in: Kurz, W., Wibberley, C., Collettini, C., Holdsworth, B., Imber, J. (Eds.), The internal structure of fault zones: fluid flow and mechanical properties. Geological Society, London, Special Publications.

Renshaw, C.E., 1996. Influence of subcritical fracture growth on the connectivity of fracture networks. Water Resources Reseach 32, 1519–1530.

Scholz, C.H., Cowie, P.A., 1990. Determination of total strain from faulting using slip measurements. Nature 346, 837–839.

Schöpfer, M.P.J., Childs, C., Walsh, J.J., 2006. Localisation of normal faults in multilayer sequences. Journal of Structural Geology 28, 816–833.

Segall, P., Pollard, D.D., 1983. Joint formation in granitic rock of the Sierra Nevada. Geological Society of America Bulletin 94, 563–575.

Shipton, Z.K., Cowie, P.A., 2001. Damage zone and slip-surface evolution over m to km scales in high-porosity Navajo sandstone. Journal of Structural Geology 23, 1825–1844.

Stephens, M., 1965. The goodness-of-fit statistic VN: distribution and significance points. Biometrika 52, 309–321.

Taylor, W.L., Pollard, D.D., Aydin, A., 1999. Fluid flow in discrete joint sets: field observations and numerical simulations. Journal of Geophysical Research 104, 28983–29006.

Terzaghi, R.D., 1965. Sources of errors in joint trace surveys. Geotechniques 15, 287–304.

Underhill, J.G., Stoneley, R.C., 1998. Introduction to the development, evolution and petroleum geology of the Wessex Basin, vol. 133. Geological Society, London. Special Publications, 1-18.

Vermilye, J.M., Scholz, C.H., 1995. Relation between vein length and aperture. Journal of Structural Geology 17, 423–434.

Whittaker, A., Green, G.W., 1983. Geology of the Country Around Weston-super-Mare, Sheet 279 and parts of 263 and 295. Memoir of the Geological Survey of Great Britain.